Tanskanen, Anne; Sundberg, Pia; Nolan, Michael; Karppinen, Maarit

Atomic/molecular layer deposition of Ti-organic thin films from different aromatic alcohol and amine precursors

Published in:
Thin Solid Films

DOI:
10.1016/j.tsf.2021.138896

Published: 31/10/2021

Document Version
Publisher's PDF, also known as Version of record

Thin Solid Films 736 (2021) 138896

Contents lists available at ScienceDirect

Thin Solid Films

journal homepage: www.elsevier.com/locate/tsf

Atomic/molecular layer deposition of Ti-organic thin films from different aromatic alcohol and amine precursors

Anne Tanskanen [a], Pia Sundberg [a], Michael Nolan [b], Maarit Karppinen [a,*]

[a] Department of Chemistry and Materials Science, Aalto University, FI-00076 Espoo, Finland
[b] Tyndall National Institute, University College Cork, Cork T12 R5CP, Ireland

A B S T R A C T

Atomic/molecular layer deposition (ALD/MLD) processes based on $TiCl_4$ as the metal source, and hydroquinone (HQ), 4-aminophenol (AP), p-phenylenediamine (PDA) or 4,4′-oxydianiline (ODA) as the organic precursor are systematically investigated to shed light on the factors affecting the inorganic-organic thin film growth. All the four ALD/MLD processes yield amorphous Ti-organic thin films which are here characterized by ex-situ X-ray reflectivity and Fourier transform infrared measurements for the film thickness and bonding scheme. First principles modelling results are presented to explore differences in the interaction of organic precursors with surface-bound $TiCl_4$. For the $TiCl_4$+AP process the high growth rate achieved, i.e. ca. 10 Å per one ALD/MLD cycle, essentially corresponds to the ideal thickness of the [Ti-O-C_6H_4—N-Ti] building unit. For both the ODA- and PDA-based processes the growth rates are considerably lower, while the $TiCl_4$+HQ process yields the hybrid film with an intermediate growth rate. We attribute these observations to (i) the higher reactivity of the OH groups in comparison to the NH_2 groups towards $TiCl_4$, and (ii) the higher tendency of a heterobifunctional organic precursor to orientate vertically and avoid unwanted double reactions on the surface.

1. Introduction

Inorganic-organic hybrid materials have potential to possess exciting combinations of properties singly seen for inorganics or organics in conventional materials. This has stimulated the research on these intriguing materials already for years. The first commercial hybrid materials came to the markets in 1950s [1], and today they are already used in many different applications, such as optics, electronics and medicine [2]

Many of the potential high-end applications of the inorganic-organic hybrid materials require the use of high-quality thin films, putting demand on the fabrication technique employed. Atomic layer deposition (ALD) is one of the state-of-the-art thin-film techniques of industrial relevance. It is based on sequential, self-limiting surface-saturated gas-solid reactions, which makes the precise control of film thickness and composition possible [3,4]. However, the majority of the materials fabricated using ALD have been relatively simple inorganic compounds. It was in 1990s when the variant of ALD which produces organic thin films was developed [5,6]; the technique is now known as molecular layer deposition (MLD). Most importantly, the combination of ALD and MLD enables the fabrication of high-quality inorganic-organic hybrid thin films [7–10].

In Fig. 1, the sequential ALD/MLD growth of hybrid metal-organic thin films is schematically illustrated [11]; the illustration is for the prototype case where the metal precursor has two reactive ligands and the organic precursor has two functional groups. In Step 1, the metal precursor is pulsed into the reactor which then reacts with the active sites on the surface. In Step 2, inert gas is used to purge the reactor of excess precursor and possible by-products. This is followed by the second precursor pulse (Step 3), i.e. the organic precursor, after which the reactor is again purged with inert gas (Step 4). The four steps together form one ALD/MLD cycle, which is repeated until the desired film thickness is achieved. It is important to note that the scheme presented in Fig. 1 is for the ideal case; in practice many metal precursor molecules are bulky causing steric hindrance while many organic precursors are flexible and tend to tilt and react twice on the surface, i.e. through both of its functional groups. Both the steric hindrance and the unwanted double reactions decrease the number of accessible/reactive surface sites and thereby depress the film growth rate. It should be emphasized that the steric hindrance is a common phenomenon even in conventional ALD of simple inorganic thin films [4,12], while the double-surface-reaction issue has been observed in ALD/MLD when using for example ethylene glycol as the organic precursor [8,11].

Until this day there are already a wide variety of ALD/MLD processes for different hybrid inorganic-organic materials, in particular the approach has been extended – besides those of typical ALD elements (Al, Zn, Ti, Zr) – to a number of different metal components (transition metals, lanthanides, s-block elements) [14–25]. However, the variety of

* Corresponding author.
E-mail address: maarit.karppinen@aalto.fi (M. Karppinen).

https://doi.org/10.1016/j.tsf.2021.138896
Received 18 January 2021; Received in revised form 10 August 2021; Accepted 13 August 2021
Available online 18 August 2021

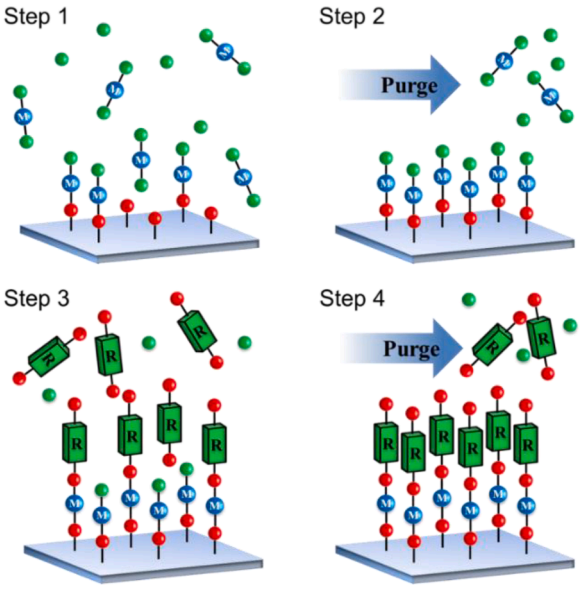

Fig. 1. The four steps of one ALD/MLD cycle to deposit inorganic-organic hybrid thin films: (1) metal precursor pulse, (2) N_2 purge, (3) organic precursor pulse, and (4) N_2 purge. Figure adapted from P. Sundberg, M. Karppinen, Eur. J. Inorg. Chem. 2014, 968–974 [13].

organic precursor types, in particular regarding their functional groups (typically homobifunctional alcohols or carboxylic acids) has remained less emphasized [26].

For the deeper insights into the ALD/MLD processes, researchers typically compare the optimized process parameters and resultant thin-film growth rates. However, such comparisons can be somewhat difficult based on data accumulated in different laboratories and/or different types of ALD reactors. Hence, we decided to systematically investigate the factors affecting the hybrid film growth using the same reactor and the same metal precursor but testing different organic precursors. We selected $TiCl_4$ for the metal source as it is stable and easily handled and one of the precursors commonly employed in conventional ALD [27], and in particular since its small Cl-ligands were considered to have less effect on the growth rate via steric hindrance compared to organometallic compounds, such as diethyl zinc (DEZ). Also, compared to e.g. DEZ with Zn in divalent state, $TiCl_4$ with tetravalent titanium provides more bonding sites. Moreover, in our preliminary tests it was found to react with all the organic precursors investigated here.

For the organic precursors, we chose four homo- or hetero-bifunctional aromatic compounds with hydroxy and/or amino groups as reactive groups, i.e. hydroquinone (HQ), 4-aminophenol (AP), p-phenylenediamine (PDA) and 4,4′-oxydianiline (ODA), see Fig. 2 for their molecular structures. Note that the stiff aromatic backbone has been considered to diminish the possibility of unwanted double reactions that hinder the film growth [11,27]. Amongst the processes investigated in this comparative study, the $TiCl_4$+AP, $TiCl_4$+ODA and $TiCl_4$+HQ processes were developed in our group [9,13,28], while the $TiCl_4$+PDA process was utilized by another group though no details of process development were given [29]. Of these four studies, only the first two were carried out using the reactor type now employed in the present study. Since the reactor type is likely to affect the growth characteristics details, we started the present study by optimizing the $TiCl_4$+HQ and $TiCl_4$+PDA processes for the present reactor. Moreover, in the case of the HQ and AP precursors, we discuss the data in comparison to the corresponding zinc-based hybrid films [30]. First principles density functional theory (DFT) simulations give further insights into the binding of the different organic functional groups and help rationalise the experimental results

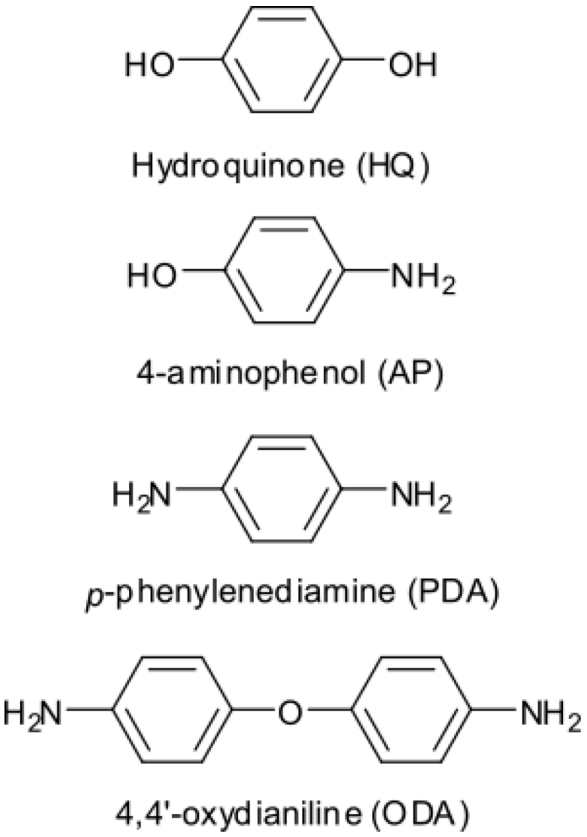

Fig. 2. Chemical structures of the organic precursors investigated: hydroquinone (HQ), 4-aminophenol (AP) molecules and p-phenylenediamine (PDA) and 4,4′-oxydianiline (ODA).

2. Experimental and computational details

All the hybrid thin films were deposited on Si(100) substrates in a commercial ALD reactor (F-120 by ASM Microchemistry Ltd.) using $TiCl_4$ (Sigma-Aldrich, ≥ 99.995 %) and diethyl zinc (DEZ; Aldrich, 52 wt % Zn) as the inorganic precursors and 4-aminophenol (AP; Alfa Aesar, 98 %), hydroquinone (HQ; Sigma-Aldrich, ≥99.5 %), 4,4′-oxydianiline (ODA; Alfa Aesar, 98 %/Fluka, >98 %) and phenylenediamine (PDA, Sigma-Aldrich, ≥99 %) as the organic precursors. $TiCl_4$ and DEZ were kept in containers outside the reactor, and AP, HQ, ODA and PDA in glass crucibles inside the reactor where they were heated at 110, 120, 150 and 95 °C, respectively. Nitrogen (>99.999 %, Schmidlin UHPN 3000 N_2 generator) was used as a carrier and purging gas.

The film thicknesses were determined from X-ray reflectivity (XRR; PANalytical X'Pert PRO MPD diffractometer; CuK_α radiation; point detector), and also from reflectance and transmittance spectra (Hitachi U-2000) measured in a wavelength region of 190–1100 nm and analysed using a procedure described in [31]. To follow the film growth characteristics, so-called growth-per-cycle (GPC) values were calculated by dividing the film thickness value by the number of ALD/MLD precursor pulsing cycles applied. Fourier transform infrared (FTIR; Nicolet Magna 750; DTGS detector; measurement chamber was purged with dry air) spectroscopy was used in a transmission mode (resolution 4 cm^{-1}) to gather information of the chemical state of the films, i.e. the presence of anticipated chemical bonds and organic groups. The spectra were measured for ca. 100 nm thick samples, and the spectrum of a clean Si substrate was subtracted from the sample spectra to deduce the substrate interference.

Periodic density functional theory (DFT) as implemented in the VASP5.4 code [32,33] was used to explore the interaction of hydroxyl-terminated HQ, amide-terminated PDA and heterobifunctional (OH,

NH_2-terminated) AP with the $TiCl_4$-modified hydroxylated anatase (101) surface. The generalised gradient approximation of Perdew-Burke-Ernzerhof (PBE) [34] was used to approximate the exchange-correlation functional. In these calculations core-valence electron interactions are described by all-electron PAW (projector augmented wave) potentials [35,36], with 4 electrons for Ti, 6 electrons for O, 4 electrons for C, 5 electrons for N and 1 electron for H. Plane wave cut-off energy of 400 eV is used and k-point sampling is achieved with a (2 × 2 × 1) Monkhorst-Pack k-point sampling grid [37]. Gaussian smearing is used, with a smearing of 0.1 eV. Convergence criteria are 1e-04 eV in the energy and 0.02 eV/ Å for the forces and no symmetry is applied. Calculations are spin polarised.

A surface slab orientated in the (101) direction was used to describe anatase TiO_2, with a surface supercell of dimensions 20.61 Å x 15.16 Å. The slab was modelled as 6 atomic layers which we use as a model of the typical thin TiO_2 layer that would be present in a titanium-based hybrid film, rather than a thicker surface slab typically used to represent an anatase film. On the basis of previous work, the anatase surface was modified by surface bound hydroxyl groups and we examine two coverages: the higher coverage model has a half coverage of surface hydroxyls (6 water molecules, Fig. 3), while the lower coverage model has a coverage of 10 surface hydroxyls (5 water molecules). These hydroxyls are needed for the adsorption of $TiCl_4$, which results in elimination of HCl; in this work we considered $TiCl_3$ and $TiCl_2$ species and found the former promote the formation of the Ti-O/Ti-N bonds with the organic species.

With $TiCl_3$ modified surfaces (at both hydroxyl coverages) we then explore the energetics of interaction with HQ, PDA and AP (through both –OH and $–NH_2$ terminations) to assess the stability the resulting Ti-organic structures. The interaction energy is computed from:

$$E^{int} = E(TiCl_2\text{-}X) + E(HCl) - [E(TiCl_3) + E(XH)],$$

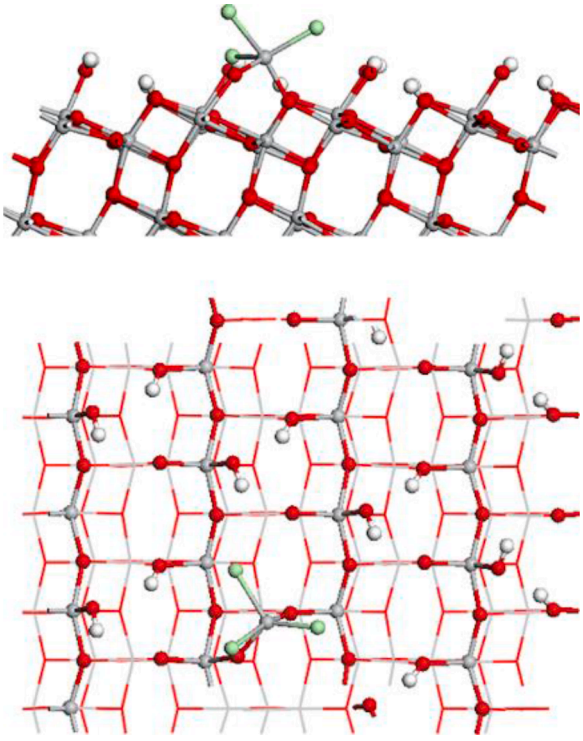

Fig. 3. Atomic structure of the model TiO_2 anatase (101) surface, terminated with surface hydroxyl groups and with a surface bound $TiCl_3$ species from the $TiCl_4$ pulse. Titanium is represented by grey spheres, oxygen by red spheres, chlorine by green spheres and hydrogen by white spheres. (For interpretation of the references to colour in this figure legend, the reader is referred to the web version of this article.)

where $E(TiCl_2\text{-}X)$ is the total energy of the hybrid system, E(XH) is the total energy of the free molecule (HQ, PDA, AP), $E(TiCl_3)$ is the total energy of the $TiCl_3$-terminated anatase (101) surface and E(HCl) is the total energy of the free HCl molecule. From the relaxed structure of the resulting $TiCl_2$-organic species, we then allow a $TiCl_4$ molecule to interact with the free end of the organic and compute the energy difference, E^{int}, in the same way. A negative value of E^{int} signifies an exothermic interaction.

3. Results and discussion

All the four $TiCl_4$-based ALD/MLD processes investigated were found to yield homogeneous Ti-organic thin films. Moreover, all the films were found to be appreciably stable in ambient conditions, remaining visually unchanged (no signs of spots or clouding) even for extended periods of storage in ordinary laboratory conditions. It should be emphasized that this is not always the case with the ALD/MLD fabricated inorganic-organic thin films [7].

3.1. Deposition temperature ranges

We started the detailed process optimizations by establishing the possible deposition temperature ranges, by observing the film quality (visual homogeneity and stability) and the process behaviour (evolution of the GPC value). In ALD and MLD, the lowest possible deposition temperature is defined by the temperature applied to evaporate the precursors (T_{prec}). Organic precursors typically require higher evaporation temperatures and are thus the limiting factors for the feasible deposition temperature range [38]. In this work, the T_{prec} values for the organic precursors were (in °C): 110 (AP), 120 (HQ), 150 (ODA) and 95 (PDA). The precursor pulse lengths in these initial experiments were chosen based on preliminary tests/previous experience on related processes to be: 1.5 s for $TiCl_4$, 20 s for HQ, 5 s for AP, 15 s for PDA and 14 s for ODA [9,13]. However, these choices turned out to be quite close to the values required for the full surface saturation, determined in later experiments. The length of the N_2 purge was chosen to be the same as the precursor pulse (except for the shortest precursor pulses in which case the purge length was twice the precursor pulse length).

For the $TiCl_4$+HQ (T_{prec} = 120 °C) process the deposition experiments could be started from 130 °C; with increasing temperature the GPC value decreased gradually from 4.3 Å/cycle at 130 °C to ~2 Å/cycle at 325 °C. For AP, T_{prec} was 110 °C, and the $TiCl_4$+AP deposition experiments were started from 120 °C. Hybrid Ti-AP films were obtained up to 220 °C, but the quality of the films began to deteriorate after 160 °C [13]. Also, the highest GPC values, i.e. 10–11 Å/cycle, were achieved in the temperature range between 120 and 160 °C. Depositions with PDA could be started already from 110 °C because of the low T_{prec} value of 98 °C. However, the Ti-PDA films grown at temperatures below 300 °C were not fully stable (judged from the immediate colour change seen after removing the films from the reactor); at 300 °C visually stable and uniform films were obtained. For the $TiCl_4$+ODA process the lowest possible deposition temperature was 160 °C (T_{prec} = 150 °C), and visually homogeneous films were obtained even up to the amazingly high temperature of 490 °C [9]. When deposited in the lower temperature range of 160–230 °C, the initially shiny films started to gradually dim (presumably due to Cl impurity reacting with humid air), while no changes were observed for the films deposited at 250 °C and above. All the Ti-ODA films retained the thickness for several months. Note that in our early work on the Ti-ODA films [9], the Cl-content was examined as a function of deposition temperature by XRF, and with increasing deposition temperature the Cl-content was found to decrease.

Fig. 4 summarizes the dependency of the GPC value on the deposition temperature for all the four ALD/MLD processes investigated. For the two diamine-based films, Ti-ODA and Ti-PDA, the GPC increases when temperature is increased whereas in the case of Ti-AP (hetero-bifunctional) and Ti-HQ (dihydroxyl-functional) the GPC value decreases

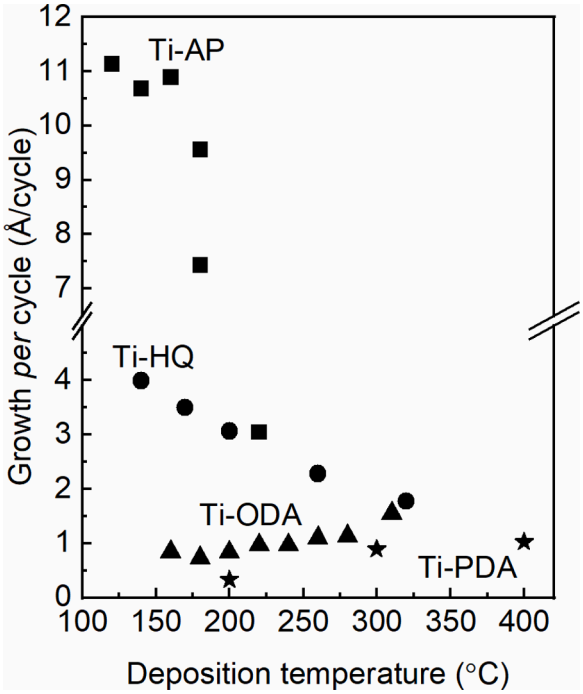

Fig. 4. Deposition temperature profiles for the four Ti-organic ALD/MLD processes investigated.

when temperature is increased. For conventional ALD processes, such an increase in GPC with increasing deposition temperature as seen here for the $TiCl_4$+ODA and $TiCl_4$+PDA processes is often explained by either (i) precursor decomposition, or (ii) need to overcome a high reaction energy barrier [39]. These two phenomena are typically differentiated from each other by means of detailed surface-reaction saturation experiments and/or FTIR spectroscopy. In the first case (decomposition), the film growth does not saturate and the FTIR spectrum is likely to show additional features due to unwanted decomposition products. In the second case (reaction barrier) surface saturation is reached with sufficient precursor pulse lengths and the FTIR spectrum is free from additional peaks.

For the present Ti-PDA and Ti-ODA films, no features that would indicate decomposition were seen in the FTIR spectra, recorded in the case of Ti-PDA for a film deposited at 300 °C and in the case of Ti-ODA for a film deposited at 290 °C [9]; the FTIR spectra are discussed later in more detail. Also, the GPC values saturated by increasing the precursor pulse lengths. Hence, we tentatively conclude that for the diamines (with amino groups) the reaction energy barrier is considerably higher than for the diols (with hydroxy groups). However, it should be mentioned that for a Ti-PDA film deposited at 400 °C the FTIR spectrum already revealed some changes possibly indicating towards decomposition, even though the film still looked visually good.

For the $TiCl_4$+HQ and $TiCl_4$+AP processes the GPC value decreases with increasing deposition temperature (in the latter case more steeply). This trend could be attributed to a temperature-dependant number of reactive sites on the surface. For example, due to their very low vapour pressures organic precursors may stick/adsorb on the film surface to act as extra surface sites in the lower temperature regime [40,41].

3.2. Surface saturated growth

Based on the afore-described temperature profiles we then fixed the deposition temperatures for the rest of the experiments as follows: 170 °C for Ti-HQ, 140 °C for Ti-AP, 300 °C for Ti-PDA and 310 °C for Ti-ODA. At these temperatures the processes were believed to work in an essentially ideal manner. This was then confirmed by investigating the film growth saturation upon increasing the precursor pulse lengths, specifically at these fixed deposition temperatures. For an ideal ALD/MLD process, the GPC value is expected to settle into a kind of plateau upon increasing the precursor pulse lengths, and the starting point of this plateau is considered to be the pulse length that is sufficient for the saturated film growth. In our previous works for the $TiCl_4$+AP and $TiCl_4$+ODA processes [9,13], it was noticed that the use of longer pulse lengths than 1.5 s for $TiCl_4$ resulted in lower GPC values, presumably due to adsorption of excess chlorine on the surface with unnecessarily long $TiCl_4$ pulses. Thus, in the present study the $TiCl_4$ pulse length was fixed to 1.5 s, and only the organic precursor pulse lengths were varied. From Fig. 5, the point where the GPC value does not increase anymore is reached for all the four processes. The pulse length required for this varies significantly amongst the four organic precursors, being 15 s for HQ, 7 s for AP, 25 s for PDA and 12 s for ODA. The exceptionally long pulse length required in the case of PDA is an indicative of the low reactivity of the precursor as already discussed based on the deposition temperature profile data.

In Fig. 6 we summarize the optimized process parameters (deposition temperatures and pulse lengths) for the four Ti-organic processes investigated. For the hydroxyl-homofunctionalized HQ, the saturation (170 °C) GPC value of 3.7 Å/cycle is little higher than the earlier reported value of 3.1 Å/cycle [28]. With the amino-homofunctionalized PDA and ODA precursors the saturation (300 °C) GPC values are 1.2 and 1.5 Å/cycle, respectively. The latter value is higher than in our previous work for Ti-ODA (ca. 0.62 Å/cycle) [9], presumably due to the (too) long $TiCl_4$ pulse time (GPC decreases with higher pulse time) used in our original study. For both the diamine-based processes, $TiCl_4$+PDA and $TiCl_4$+ODA, the lower reactivity of the amino groups with $TiCl_4$ in comparison to the hydroxyl groups is believed to be the main reason for the lower GPCs. Here we should also recall the fact that relatively long pulses were required to achieve the full surface coverage in the cases of the two amino-homo-functionalized precursors. The ODA molecule moreover has two aromatic rings, a fact that makes it relatively bulky. Moreover, the molecule is prone to bend from the ether bond between the rings. Both of these features increase the steric hindrance and enhance the probability of the unwanted double surface reactions that could explain the lower growth rate in its case, but not for the smaller PDA molecule.

The most interesting comparison is between the organic precursors with a single aromatic ring (HQ, AP, and PDA); amongst them the hetero-bi-functionalized AP with both hydroxyl and amino groups yields the clearly highest saturation GPC values, even up to 10~11 Å/cycle (140 °C). Noteworthy, these values are close to the value estimated based on the anticipated bond lengths for a straight Ti-AP chain, i.e. 9.1 Å per cycle [13]. The size of the AP molecule cannot explain the high growth rate, as the HQ and PDA molecules are more or less of the same size as AP. Instead, we suggest that in the case of a heterobifunctional precursor for which one of the groups is more reactive (OH) than the other (NH_2), the unwanted double surface reactions are efficiently reduced.

3.3. Computational modelling

To support this suggestion, we used periodic DFT within the PBE exchange-correlation functional to examine the differences in interaction strength between the hydroxyl terminated HQ, amine terminated PDA and the heterobifunctional AP. Fig. 7 shows the atomic structure of the lowest energy configurations obtained for HQ, PDA and AP upon interaction at surface bound $TiCl_3$ at half coverage of surface hydroxyls; similar results were found for the lower hydroxyl coverage as well (not shown here). The computed interaction energies are: −1.1 eV and −1.38 eV for HQ and PDA, while for AP the energies are −1.50 eV and −1.12 eV for the interaction through O and N, respectively. These are all accompanied by formation of HCl. Thus, in the heterobifunctional AP, there is a clear difference between the stability when binding through

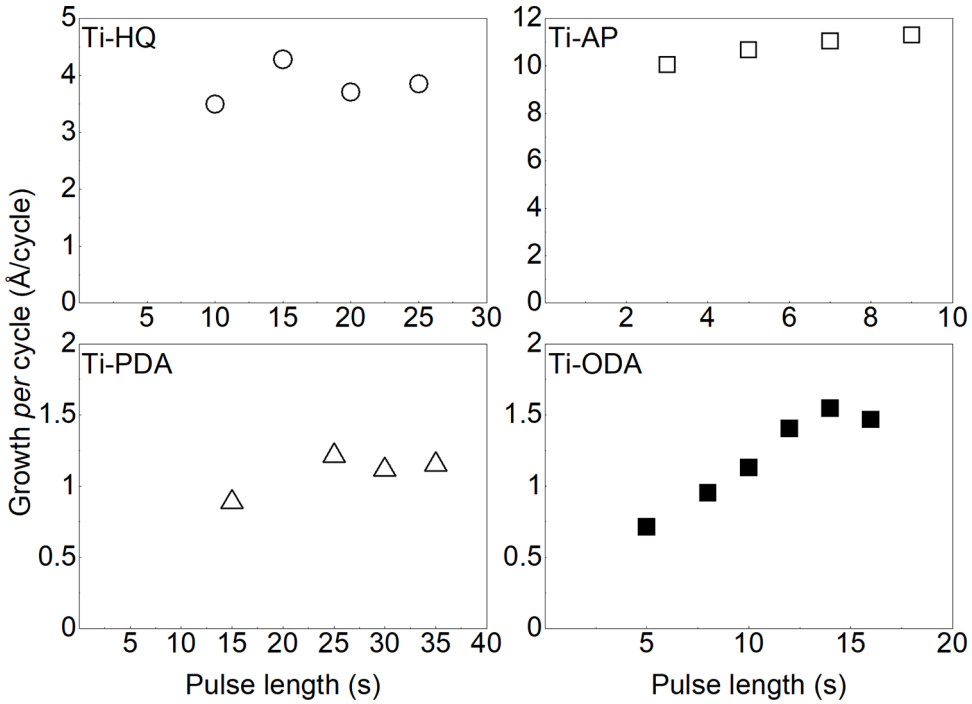

Fig. 5. GPC versus organic precursor pulse length curves showing the saturation behaviour for the four Ti-organic processes investigated.

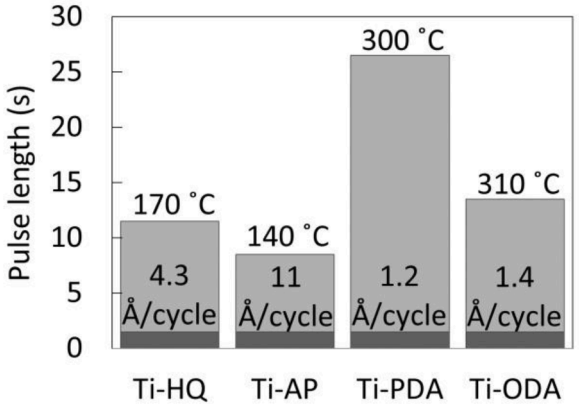

Fig. 6. Summary of pulse lengths required to achieve surface saturation and the maximal GPC value for the four Ti-organic ALD/MLD processes investigated at the given deposition temperature: the $TiCl_4$ pulse was fixed for all the processes to 1.5 s (the dark grey pillars at the bottom) while the light grey pillars on the top represent the pulse lengths of the organic precursors.

the OH and the NH_2 sites, with the former being preferred. It is also interesting to see that the interaction of Ti with the amide site of PDA is stronger than with the oxygen site of HQ. In all cases though, the energy difference is exothermic, which is consistent with deposition of the MLD films.

The Ti-O distances in HQ and AP are 2.05 and 2.02 Å, while the Ti-N distances in PDA and AP are 2.12 and 2.16 Å. The Ti-O distances are longer than those in the corresponding oxide, while the Ti-N distances are close to those of bulk TiN (2.12 Å) [42].

We also considered the second half reaction, namely the interaction of the –OH/–NH_2 end of the organic molecule with a $TiCl_4$ precursor; the atomic structures are shown in Fig. 8. In all cases, HCl is eliminated and a Ti-O/Ti-N bond is formed. The resulting overall energy change for the two reactions is exothermic and is −0.97 eV for HQ, −0.63 eV for PDA, −0.63 eV for AP through the hydroxyl site and −1.01 eV through the amide site. Thus, we see that the most favourable situation is for the AP molecule to bind through the hydroxyl to the original $TiCl_4$ precursor, while its amide group reacts with the next $TiCl_4$ precursor. This should promote an upright bonding configuration of the AP precursor.

3.4. Chemical bonding structure

All the films grown were amorphous and thus diffraction techniques could not be used to examine the structures of the films. Therefore, we employed FTIR spectroscopy to verify the intended organic components in our Ti-HQ, Ti-AP, Ti-PDA and Ti-ODA films and to investigate the chemical bonding structure. For all the films features due to the aromatic (Ar) ring(s) and hydroxyl and/or amino groups were seen, as expected. In Fig. 8, we compare the FTIR spectra for the present Ti-organic films with corresponding zinc-based thin films of Zn-HQ [43] and Zn-AP [30], grown in this study just for a reference. The Zn-HQ film in particular is an excellent reference as its FTIR spectrum has been well explained on the bases of both experimental and computational data [44]: the features due to the Zn-O bonds are seen around 500 cm^{-1}, while the footprints related to the Ar ring are the strong sharp peak around 1500 cm^{-1} ($C = C$ stretching) and the less intense peaks around 1200 cm^{-1} (C—H in-plane bending coupled with C—O stretching) and 800 cm^{-1} (C—H out-of-plane bending). These main features are also now seen for the present Ti-HQ, Ti-AP and Ti-PDA films, as well as the other Zn-based reference, Zn-AP.

From Fig. 9, for all the films based on the amine-functionalized organic precursors (AP, ODA and PDA) weak peaks in the N—H region around 3300 cm^{-1} are seen, as expected. For Ti-PDA the peak is broad and slightly stronger than for the other films. Peaks due to the metal (M = Ti or Zn) related M-O and M-N bonds are all seen below 500 cm^{-1}. Also, as chlorine is a common impurity in ALD and ALD/MLD films grown from metal chloride precursors, it is possible that some of these peaks contain contributions from Ti-Cl bonds as well [45]. The peak in the 1200 cm^{-1} area ($C = C$/C—O or $C = C$/C—N stretch) is broader for Ti-AP and Zn-AP compared to Ti-HQ and Zn-HQ. The broader peak is an indication of overlapping bands that means more variation in bonding types for the AP-based films.

The area around 800–1000 cm^{-1} seems to be quite sensitive to the differences in the bonding schemes. In the case of Zn-based films, only

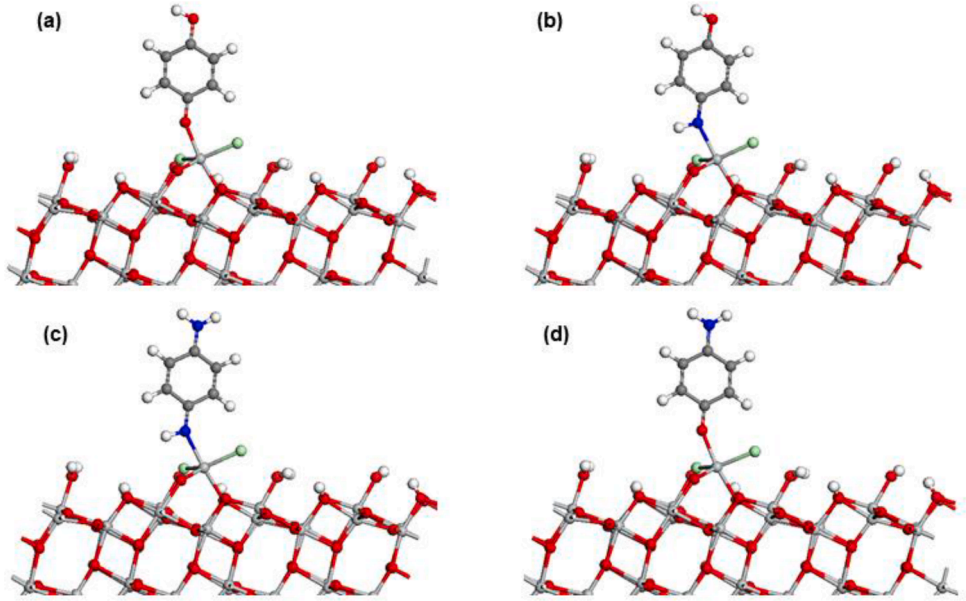

Fig. 7. Atomic structures for the interaction of the organics with $TiCl_3$-terminated anatase (101) (in all reactions, HCl has been released): **(a)** HQ; **(b)** AP through nitrogen; **(c)** PDA; **(d)** AP through oxygen. Ti is the light grey sphere, C is the dark grey sphere, O is the red sphere, N is the blue sphere, Cl is the green sphere and H is the white sphere. (For interpretation of the references to colour in this figure legend, the reader is referred to the web version of this article.)

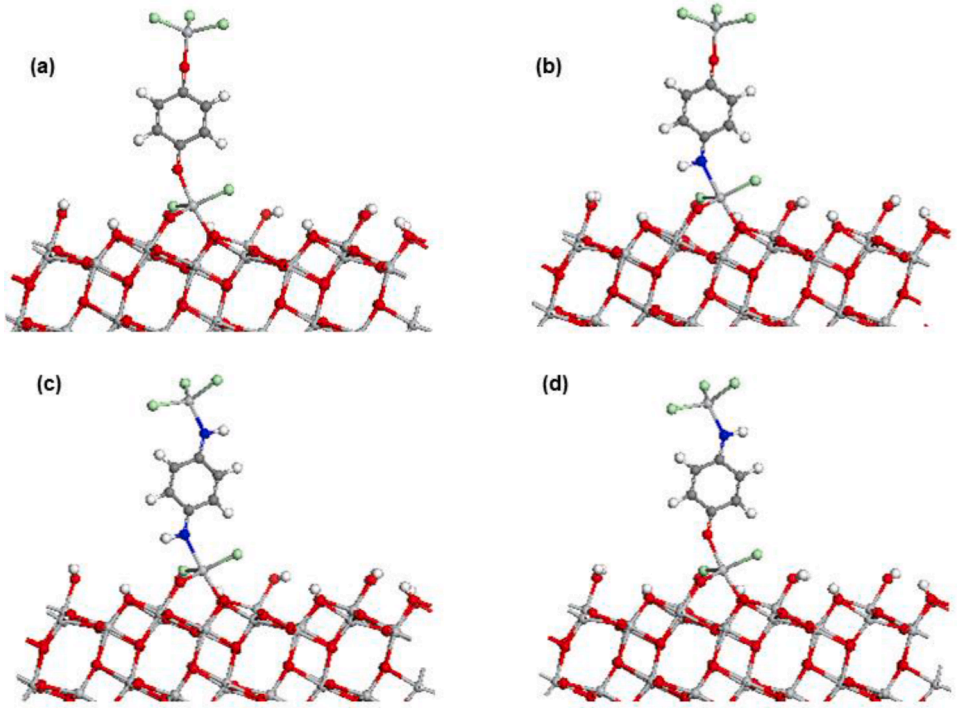

Fig. 8. Atomic structures for the interaction of $TiCl_4$ in the second half-cycle with the organic species in Fig. 6 (in all reactions, HCl has been released: **(a)** HQ; **(b)** AP through oxygen; **(c)** PDA; **(d)** AP through nitrogen. Figure colours are the same as Fig. 7.

two bands are seen for both Zn-HQ and Zn-AP, but the distance between these bands varies, being longer for Zn-AP. For the corresponding Ti-based films, Ti-HQ and Ti-AP, somewhat similar sets of two bands are seen, but for Ti-AP an additional band is seen at a lower wavenumber. We believe that the fact that three bands are seen for Ti-AP while only two for Zn-AP (as an indication of different bonding schemes in these films), is rather understandable taking into account the different charges/sizes of the Ti^{4+} and Zn^{2+} ions.

Finally, to summarize our findings for the film growth characteristics and the chemical bonding schemes, Fig. 10 illustrates the structure of our Ti-AP thin films with a simple 2D schematic. From the DFT results, the AP precursor molecule can bind to the Ti^{4+} ions via both the OH and NH_2 groups leading to both Ti-O and Ti-N bonds in the hybrid film structure. The result that the OH group reacts more strongly than the NH_2 groups with $TiCl_4$ on the surface may promote some degree of ordering of the Ti-O and Ti-N bonded layers, as indicated in the schematic structure.

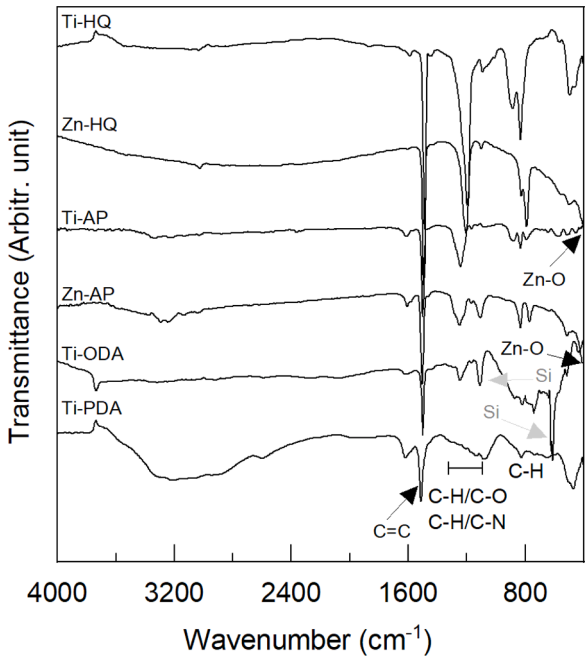

Fig. 9. FTIR spectra for the four Ti-organic films investigated, together with those for Zn-HQ and Zn-AP reference films.

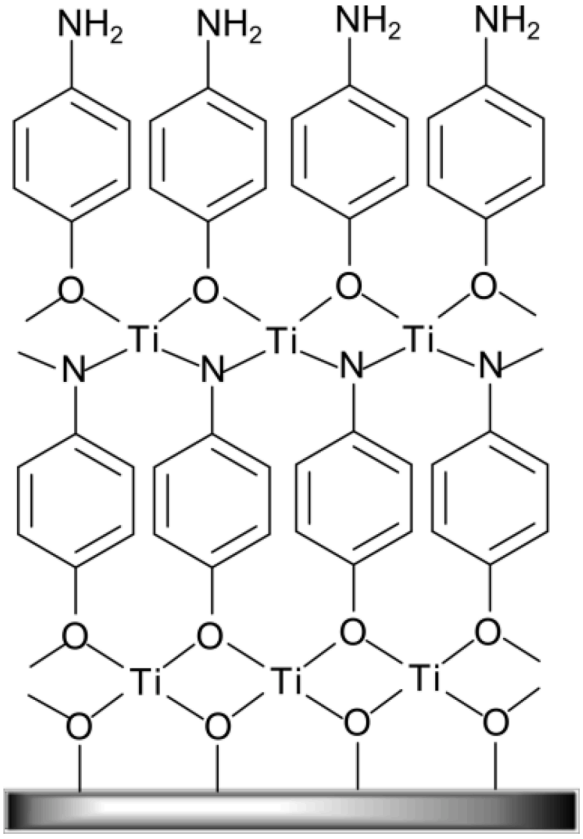

Fig. 10. 2D schematics of the suggested (ideal) bonding structure in the hybrid Ti-AP films. This structure is based on the finding that the OH site in AP is more reactive towards $TiCl_4$ than the NH_2 site.

4. Conclusions

In this paper we have discussed the role of the reactive/functional groups of the organic precursor in the ALD/MLD growth of inorganic-organic hybrid thin films. The four different organic precursors selected for this study were all bifunctional, possessing different combinations of hydroxy and amino groups as the reaction sites; the organic precursors were: homobifunctional hydroquinone (HQ) with hydroxy groups only, heterobifunctional 4-aminophenol (AP), and homobifunctional *p*-phenylenediamine (PDA) and 4,4′-oxydianiline (ODA) with amino groups only. As the metal precursor, $TiCl_4$ was employed. The advantage of $TiCl_4$ over the other common metal precursors were its relatively small chlorine ligands (not to pose significant steric hindrance effects), and the high valent titanium (to provide enough bonding sites).

All the four different organic precursors yielded – in a well-controlled manner – hybrid thin films when combined with $TiCl_4$, as intended. The resultant Ti-AP, Ti-HQ, Ti-PDA and Ti-ODA films were all amorphous, and thus we investigated their bonding structures using FTIR spectroscopy. For this comparison we also included the data obtained by us under similar conditions for the two zinc-based hybrid thin films, Zn-HQ and Zn-AP. Such a comparison enabled us to identify and discuss the spectral features in detail, to provide also a useful platform for discussing the FTIR spectra for similar/related hybrid thin films in future with other metal constituents.

Intriguing results concerned the reactivities and growth rates achieved with the different organic precursors. The amino-functional precursors, PDA and ODA, were found clearly less reactive (reacting better with increasing deposition temperature) than the precursors having hydroxy groups. Most excitingly, these different reactivities of the OH and NH_2 groups were shown to be rather useful, when combined into a single heterofunctional precursor molecule. Namely, we observed the clearly highest growth rates for the Ti-AP films, and tentatively attributed this to the lessening the probability of the unwanted double surface reactions, as each AP molecule preferred to react on the Ti-Cl surface through its OH group (leaving the NH_2 group unbonded until the next $TiCl_4$ precursor was pulsed into the reactor chamber) or because of the more vertical orientation of the hetero-functionalized organic molecules.

CRediT authorship contribution statement

Anne Tanskanen: Conceptualization, Investigation, Visualization, Writing – original draft. **Pia Sundberg:** Investigation. **Michael Nolan:** Investigation, Writing – original draft. **Maarit Karppinen:** Supervision, Resources, Funding acquisition, Writing – original draft.

Declaration of Competing Interest

The authors declare that they have no known competing financial interests or personal relationships that could have appeared to influence the work reported in this paper

Acknowledgements

This work has received funding from the Academy of Finland (296299) and the European Research Council under the European Union's Seventh Framework Programme (FP/2007–2013)/ERC Advanced Grant Agreement (339478). M.N. acknowledges support from Science Foundation Ireland through the SFI-NSF China Partnership project NITRALD (17/NSFC/5279) and from the SFI/HEA-funded Irish Centre for High End Computing, ICHEC. The experimental research made use of the RawMatters Finland infrastructure (RAMI) facilities based at Aalto University.

References

[1] B. Arkles, Commercial applications of sol-gel-derived hybrid materials, MRS Bull. 26 (2001) 402–408, https://doi.org/10.1557/mrs2001.94.

[2] C. Sanchez, P. Belleville, M. Popall, L. Nicole, Applications of advanced hybrid organic–inorganic nanomaterials: from laboratory to market, Chem. Soc. Rev. 40 (2011) 696, https://doi.org/10.1039/c0cs00136h.

[3] T. Suntola, Atomic layer epitaxy, Mater. Sci. Rep. 4 (1989) 261–312, https://doi.org/10.1016/S0920-2307(89)80006-4.

[4] S.M. George, Atomic layer deposition: an overview, Chem. Rev. 110 (2010) 111–131, https://doi.org/10.1021/cr900056b.

[5] T. Yoshimura, S. Tatsuura, W. Sotoyama, Polymer films formed with monolayer growth steps by molecular layer deposition, Appl. Phys. Lett. 59 (1991) 482–484, https://doi.org/10.1063/1.105415.

[6] A. Kubono, N. Yuasa, H.-L. Shao, S. Umemoto, N. Okui, In-situ study on alternating vapor deposition polymerization of alkyl polyamide with normal molecular orientation, Thin Solid Films 289 (1996) 107–111, https://doi.org/10.1016/S0040-6090(96)08913-4.

[7] O. Nilsen, K. Klepper, H. Nielsen, H. Fjellvåg, Deposition of organic-inorganic hybrid materials by atomic layer deposition, ECS Trans. 16 (2008) 3–14, https://doi.org/10.1149/1.2979975.

[8] A.A. Dameron, D. Seghete, B.B. Burton, S.D. Davidson, A.S. Cavanagh, J. A. Bertrand, S.M. George, Molecular layer deposition of alucone polymer films using trimethylaluminum and ethylene glycol, Chem. Mater. 20 (2008) 3315–3326, https://doi.org/10.1021/cm7032977.

[9] A. Sood, P. Sundberg, J. Malm, M. Karppinen, Layer-by-layer deposition of Ti–4,4-oxydianiline hybrid thin films, Appl. Surf. Sci. 257 (2011) 6435–6439, https://doi.org/10.1016/j.apsusc.2011.02.022.

[10] X. Meng, An overview of molecular layer deposition for organic and organic-inorganic hybrid materials: mechanisms, growth characteristics, and promising applications, J. Mater. Chem. A 5 (2017) 18326–18378, https://doi.org/10.1039/c7ta04449f.

[11] P. Sundberg, M. Karppinen, Organic and inorganic-organic thin film structures by molecular layer deposition: a review, Beilstein J. Nanotechnol. 5 (2014) 1104–1136, https://doi.org/10.3762/bjnano.5.123.

[12] R.L. Puurunen, Formation of metal oxide particles in atomic layer deposition during the chemisorption of metal chlorides: a review, Chem. Vap. Depos. 11 (2005) 79–90, https://doi.org/10.1002/cvde.200400021.

[13] P. Sundberg, M. Karppinen, Organic–inorganic thin films from $TiCl_4$ and 4-aminophenol precursors: a model case of ALD/MLD hybrid-material growth? Eur. J. Inorg. Chem. (2014) 968–974, https://doi.org/10.1002/ejic.201301560.

[14] M. Vähä-Nissi, P. Sundberg, E. Kauppi, T. Hirvikorpi, J. Sievänen, A. Sood, M. Karppinen, A. Harlin, Barrier properties of Al_2O_3 and alucone coatings and nanolaminates on flexible biopolymer films, Thin Solid Films 520 (2012) 6780–6785, https://doi.org/10.1016/j.tsf.2012.07.025.

[15] A. Tanskanen, M. Karppinen, Iron-based inorganic-organic hybrid and superlattice thin films by ALD/MLD, Dalt. Trans. 44 (2015) 19194–19199. http://pubs.rsc.org/en/Content/ArticleLanding/2015/DT/C5DT02488A.

[16] J.P. Niemelä, N. Rohbeck, J. Michler, I. Utke, Molecular layer deposited alucone thin films from long-chain organic precursors: from brittle to ductile mechanical characteristics, Dalt. Trans. 49 (2020) 10832–10838, https://doi.org/10.1039/d0dt02210a.

[17] R.M. Silva, L.D. Carlos, J. Rocha, R.F. Silva, Luminescent thin films of Eu-bearing UiO-66 metal organic framework prepared by ALD/MLD, Appl. Surf. Sci. 527 (2020), 146603, https://doi.org/10.1016/j.apsusc.2020.146603.

[18] K.B. Lausund, O. Nilsen, All-gas-phase synthesis of UiO-66 through modulated atomic layer deposition, Nat. Commun. 7 (2016) 13578, https://doi.org/10.1038/ncomms13578.

[19] E. Ahvenniemi, M. Karppinen, In situ atomic/molecular layer-by-layer deposition of inorganic−organic coordination network thin films from gaseous precursors, Chem. Mater. 28 (2016) 6260–6265, https://doi.org/10.1021/acs.chemmater.6b02496.

[20] K. Van De Kerckhove, F. Mattelaer, J. Dendooven, C. Detavernier, Molecular layer deposition of "vanadicone", a vanadium-based hybrid material, as an electrode for lithium-ion batteries, Dalt. Trans. 46 (2017) 4542–4553, https://doi.org/10.1039/c7dt00374a.

[21] Z. Giedraityte, M. Tuomisto, M. Lastusaari, M. Karppinen, Three- and two-photon NIR-to-vis (Yb,Er) upconversion from ALD/MLD fabricated molecular hybrid thin films, ACS Appl. Mater. Interfaces 10 (2018) 8845–8852, https://doi.org/10.1021/acsami.7b19303.

[22] C. MacIsaac, J.R. Schneider, R.G. Closser, T.R. Hellstern, D.S. Bergsman, J. Park, Y. Liu, R. Sinclair, S.F. Bent, Atomic and molecular layer deposition of hybrid Mo-thiolate thin films with enhanced catalytic activity, Adv. Funct. Mater. 28 (2018), 1800852, https://doi.org/10.1002/adfm.201800852.

[23] A. Tanskanen, M. Karppinen, Iron-terephthalate coordination network thin films through in-situ atomic/molecular layer deposition, Sci. Rep. 8 (2018), https://doi.org/10.1038/s41598-018-27124-7.

[24] A. Khayyami, A. Philip, M. Karppinen, Atomic/molecular layer deposited iron–azobenzene framework thin films for stimuli-induced gas molecule capture/release, Angew. Chem. Int. Ed. 131 (2019) 13534–13538, https://doi.org/10.1002/ange.201908164.

[25] D. Choudhury, G. Rajaraman, S.K. Sarkar, Comparison on atomic/molecular layer deposition grown aluminum alkoxide polymer films using alkane and alkyne organic precursors, J. Vac. Sci. Technol. A 36 (2018) 01A108, https://doi.org/10.1116/1.4990776.

[26] A. Muriqi, M. Nolan, First principles study of reactions in alucone growth: the role of the organic precursor, Dalt. Trans. 49 (2020) 8710–8721, https://doi.org/10.1039/d0dt01376e.

[27] J.P. Niemelä, G. Marin, M. Karppinen, Titanium dioxide thin films by atomic layer deposition: a review, Semicond. Sci. Technol. 32 (2017), 093005, https://doi.org/10.1088/1361-6641/aa78ce.

[28] J.-P. Niemelä, M. Karppinen, Tunable optical properties of hybrid inorganic–organic $[(TiO_2)_m(Ti–O–C_6H_4–O–)_k]_n$ superlattice thin films, Dalt. Trans. 44 (2015) 591–597, https://doi.org/10.1039/C4DT02550D.

[29] G.-.S. Han, D.-S. Yang, S.-J. Kim, M.-M. Seong, Molecular layer deposition of titanium nitride cross-linked benzene using titaniumchloride and 1,4-phenylenediamine, in: Proc. Korean Vac. Soc. Conf., KoreaScience, 2012, p. 305.

[30] A. Sood, P. Sundberg, M. Karppinen, ALD/MLD of novel layer-engineered Zn-based inorganic-organic hybrid thin films using heterobifunctional 4-aminophenol as an organic precursor, Dalt. Trans. 42 (2013) 3869–3875, https://doi.org/10.1039/c2dt32630b.

[31] M. Ylilammi, T. Ranta-aho, Optical determination of the film thicknesses in multilayer thin film structures, Thin Solid Films 232 (1993) 56–62, https://doi.org/10.1016/0040-6090(93)90762-E.

[32] G. Kresse, J. Furthmüller, Efficiency of ab-initio total energy calculations for metals and semiconductors using a plane-wave basis set, Comput. Mater. Sci. 6 (1996) 15–50, https://doi.org/10.1016/0927-0256(96)00008-0.

[33] G. Kresse, J. Furthmüller, Efficient iterative schemes for ab initio total-energy calculations using a plane-wave basis set, J. Phys. Chem. A 54 (1996) 11169–11186, https://doi.org/10.1021/acs.jpca.0c01375.

[34] J.P. Perdew, K. Burke, M. Ernzerhof, Generalized gradient approximation made simple, Phys. Rev. Lett. 77 (1996) 3865–3868, https://doi.org/10.1103/PhysRevLett.77.3865.

[35] G. Kresse, D. Joubert, From ultrasoft pseudopotentials to the projector augmented-wave method, Phys. Rev. B 59 (1999) 1758–1775, https://doi.org/10.1103/PhysRevB.59.1758.

[36] P.E. Blöchl, Projector augmented-wave method, Phys. Rev. B 50 (1994) 17953–17979, https://doi.org/10.1103/PhysRevB.50.17953.

[37] H.J. Monkhorst, D. Pack, James, Special points for Brillouin-zone integrations, Phys. Rev. B 13 (1976) 5188–5192, https://doi.org/10.1039/c8ta11250a.

[38] J. Multia, A. Khayyami, J. Heiska, M. Karppinen, Low-pressure thermogravimetric analysis for finding sublimation temperatures for organic precursors in atomic/molecular layer deposition, J. Vac. Sci. Technol. A 38 (2020), 052406, https://doi.org/10.1116/6.0000345.

[39] R.L. Puurunen, Surface chemistry of atomic layer deposition: a case study for the trimethylaluminum/water process, J. Appl. Phys. 97 (2005), 121301, https://doi.org/10.1063/1.1940727.

[40] N.M. Adamczyk, A.A. Dameron, S.M. George, Molecular layer deposition of poly(p-phenylene terephthalamide) films using terephthaloyl chloride and p-phenylenediamine, Langmuir 24 (2008) 2081–2089, https://doi.org/10.1021/la7025279.

[41] K.B. Klepper, O. Nilsen, H. Fjellvåg, Deposition of thin films of organic-inorganic hybrid materials based on aromatic carboxylic acids by atomic layer deposition, Dalt. Trans. 39 (2010) 11628–11635, https://doi.org/10.1039/c0dt00817f.

[42] F. Mehmood, R. Pachter, N.R. Murphy, W.E. Johnson, Electronic and optical properties of titanium nitride bulk and surfaces from first principles calculations, J. Appl. Phys. 118 (2015), 195302, https://doi.org/10.1063/1.4935813.

[43] B. Yoon, B.H. Lee, S.M. George, Molecular layer deposition of flexible, transparent and conductive hybrid organic-inorganic thin films, ECS Trans 41 (2011) 271–277, https://doi.org/10.1149/1.3633677.

[44] A.J. Karttunen, T. Tynell, M. Karppinen, Atomic-level structural and electronic properties of hybrid inorganic-organic ZnO:hydroquinone superlattices fabricated by ALD/MLD, J. Phys. Chem. C 119 (2015) 13105–13114, https://doi.org/10.1021/acs.jpcc.5b03433.

[45] N.J. Hawkins, D.R. Carpenter, Force constants, infrared spectrum, and thermodynamic properties of $TiCl_4$, J. Chem. Phys. 23 (1955) 1700–1702, https://doi.org/10.1063/1.1742414.